Original Article

TJPS
The Thai Journal of Pharmaceutical Sciences
39 (4), October - December 2015: 171-179

Protein-Protein Docking and Molecular Dynamics Simulations Elucidated Binding Modes of FUBI-p62 UBA Complex

Sumet Chongruchiroj[1], Panida Kongsawadworakul[2], Veena Nukoolkarn[3], Montree Jaturanpinyo[4], Wichit Nosoong-noen[5], Jiraporn Chingunpitak[6], Jaturong Pratuangdejkul[1,*]

[1]Department of Microbiology, Faculty of Pharmacy, Mahidol University, Bangkok 10400, Thailand
[2]Department of Plant Science, Faculty of Science, Mahidol University, Bangkok 10400, Thailand
[3]Department of Pharmacognosy, Faculty of Pharmacy, Mahidol University, Bangkok 10400, Thailand
[4]Department of Manufacturing Pharmacy, Faculty of Pharmacy, Mahidol University, Bangkok 10400, Thailand
[5]Department of Pharmacy, Faculty of Pharmacy, Mahidol University, Bangkok 10400, Thailand
[6]School of Pharmacy, Walailak University, Nakhon Si Thammarat 80161, Thailand

Abstract

The cytosolic Fau protein, a precursor of antimicrobial peptide, composes of ubiquitin-like domain FUBI at N-terminus and ribosomal protein rpS30 at C-terminus. Fau has been important in killing of intracellular *Mycobacterium tuberculosis* infection through autophagy-targeting p62 mechanism. The p62 adapter protein delivered microbicidal protein rpS30 to autolysosome where it was converted into antimicrobial peptides capable of killing *M. tuberculosis* in mycobacterial phagosome. Recently, direct interaction of FUBI and p62 UBA domain has been established using immunoprecipitation. In the absence of experimental complex structure of FUBI and p62 UBA, understanding of binding interaction could be extensively characterized using molecular modeling techniques. The aim of this study was to elucidate the binding mode of interaction between FUBI and p62 UBA. Based on the conserved hydrophobic binding regions of FUBI and p62 UBA domain, 334 docked poses were predicted using the ZDOCK and RDOCK protein-protein docking algorithms. Five binding modes of complex structures were clustered and only two were stable after 15 ns of molecular dynamics simulations. The binding free energy was elucidated using the MM-PBSA method and the best FUBI-p62 UBA complex was determined. The key binding residues of FUBI and p62 UBA domain were elucidated using protein interface and alanine scanning. Gly405 and Phe406 in the MGF hydrophobic area and certain residues in loop 1 and, helices 2 and 3 of the p62 UBA domain were bound with FUBI domain. The results enable us to understand how p62 and Fau interact which is a crucial step of autophagy-targeting p62 mechanism for the antimycobacterial action.

Keywords: FUBI, p62 UBA domain, Protein-protein docking, Molecular dynamic simulation, MM-PBSA, Binding energy, Alanine scanning

Correspondence to: Jaturong Pratuangdejkul, Ph.D.Department of Microbiology Faculty of Pharmacy, Mahidol University 447 Sri-Ayudhaya Rd. Ratchathewi, Bangkok, Thailand 10400
E-mail: jaturong.pra@mahidol.edu

Received: 6 May 2015
Revised: 4 June 2015
Accepted: 29 June 2015

Academic Editor: Wanchai De-Eknamkul

Introduction

Mycobacterium tuberculosis infection remains a highly significant global health problem. *M. tuberculosis* is one of the leading causes of death in infectious diseases. The key features of *M. tuberculosis* infection are avoidance of the antimicrobial mechanisms mediated by macrophage, rendering the infection and capacity of *M. tuberculosis* to survive in macrophage. *M. tuberculosis* can prevent phagosomal maturation or inhibit phagosome-lysosome fusion, which is a critical process allowing the persistent pathogens in human like macrophage parasitism [1-3]. However, some studies have shown that stimulation of

autophagy can eliminate intracellular *M. tuberculosis* [4]. Ubiquitin-derived peptides have been found in autolysosomes and exhibited mycobactericidal activity [5]. Recently, autophagy-targeting molecule p62 (SQSTM1) has been found as an important mechanism for mycobactericidal activity [6].

Autophagy is known as homeostatic system of eukaryotic cells that delivers cytoplasmic components, including proteins, various organelles and intracellular pathogens into lysosomes for degradation [7, 8]. Autophagy can eliminate intracellular pathogens, including *Salmonella* [9], *Shigella* [10], *Listeria* [11], *Streptococcus* [12], Sindbis virus [13], human immunodeficiency virus (HIV) [14] and *M. tuberculosis* [4, 5]. There are two principal ways how autophagy directly destroys intracellular microbial pathogens. First, autophagosomes directly capture free cytosol microbes that marked with poly-ubiquitin complexes through adaptor protein such as p62 and NDP52 [9, 11-13]. The pathogen was added in autophagosomes and delivered for elimination at lysosome. Second, autophagy delivers Fau protein (a precursor of rpS30 peptides which was converted into microbicidal ribosomal protein by proteolytic enzyme in autolysosome) to the phagosome of microbes such as *M. tuberculosis* phagosome through p62 autophagy adaptor proteins [6]. Interestingly, previous report suggested that the cytoplasmic proteins L30, S19 and rpS30 have microbicidal activity against bacteria [15, 16], but only rpS30 is specifically delivered via autophagy to mycobacterial phagosome [6]. The immunofluorescence microscopy and immunoprecipitation indicated that UBA domain of p62 proteins directly interact with Fau [6]. Elucidation of the molecular structure of FUBI bound to p62 UBA domain may help in understanding of the delivery mechanism of neo-antimicrobial peptides by autophagy against *M. tuberculosis.* In the absence of the x-ray crystal or NMR structures of the complex, the Fau protein has been reported a fusion protein comprising of rpS30 fused with the Ubiquitin-like domain (FUBI) at its N-terminus [17]. The chemical shift perturbation indicated that Met-Gly-Phe (MGF) motif and α-helix 3 of p62 UBA domain proteins bind directly to Leu8, Ile44 and Val70 in the hydrophobic region of ubiquitin [18]. Especially, Ile44 of ubiquitin and ubiquitin-like (UBL) proteins is known as the center interaction residue with ubiquitin binding domain (UBD) [19]. We thus hypothesize that FUBI binds to p62 UBA domain through these hydrophobic residues. Computational approaches could be employed to elucidate the interaction mechanism of protein through protein–protein docking, particularly when the crystal or NMR complex is not available.

In this study, we used the programs, ZDOCK and RDOCK implemented in Discovery Studio 3.5 (DS 3.5) [20], to determine the structure of the FUBI-p62 UBA domain complexes. The program has successfully produced high accuracy predictions for multiple protein-protein targets in the CAPRI challenge [21]. The plausible binding modes of FUBI-p62 UBA domain complex were elucidated. The complexes were optimized using molecular dynamics (MD) simulations in explicit water box and the stable structure could be obtained. Binding free energies were calculated using molecular mechanics/Poisson Boltzmann surface area (MM-PBSA) [22] to elucidate the best binding mode of FUBI-p62 UBA complex system. Finally, the residues involved in binding interaction between FUBI and p62 UBA were characterized.

Materials and Methods

Protein structures and structural analysis

The structures of FUBI (PDB code: 2L7R), ubiquitin (PDB code: 1D3Z) and p62 UBA domain (PDB code: 2RRU) were downloaded from Protein Data Bank (http://www.rcsb.org). The preparation of protein structures, analysis of sequences and 3D structures, protein-protein docking and structure visualization were performed using molecular modeling tools in the DS 3.5 software [20].

Protein-protein docking

The structure of p62 UBA domain was docked into 20 conformations of the FUBI NMR structure for improving rigid docking performance of ZDOCK [23]. ZDOCK is a rigid protein-protein docking algorithm that was developed using pairwise shape complementarity, desolvation, and electrostatic energies [24] and employs a fast Fourier transform (FFT) algorithm with 6° rotational search. For each conformation of FUBI, the 54,000 predicted complex structures were generated and re-ranked by ZRANK scoring function [25]. The top 2,000 poses with high ZRANK score were selected and then filtered based on key binding residues from sequence and structural analysis. Total predicted complex structures were clustered and refined by RDOCK which used CHARMm-based minimization to evaluate electrostatic and desolvation energies [26]. The top RDOCK-score pose of each cluster was selected for representing the binding mode of FUBI-p62 UBA complex system.

Molecular dynamics (MD) simulations

The selected FUBI-p62 UBA complexes obtained from molecular docking were optimized using MD simulations. The MD simulations were conducted using NAMD 2.7 [27]. The CHARMM27 [28] force field was applied to protein. The structure of FUBI-p62 UBA complexes was solvated in the orthorhombic box of TIP3P water molecules [29] with a 15 Å minimum box padding from any edge of the box to any protein atom. The charge of the systems was neutralized with an appropriate number of Na^+ and Cl^- counterions which were randomly placed in the simulation box to reach the human physiological saline concentration (0.15 M NaCl). The protein in TIP3P box was initially minimized by conjugate gradient method for 100,000 steps and

temperature of entire systems was increased to 310 K over 10 ps of heating steps. The 200 ps for equilibration were performed with 40 kcal/mol.Å^2 harmonic restraint of protein backbone. The production step was carried out without any constraints for 15 ns with 2 fs time steps and SHAKE algorithm [30]. The NPT ensemble at constant temperature of 310 K and pressure of 1 atm was controlled by the Langevin Nosé-Hoover method [31]. Periodic boundary conditions (PBC) were set to avoid truncation effects. A Particle Mesh Ewald (PME) method [32] was used for calculation of long-range electrostatic forces with a grid size of less than 1 Å in all dimensions. The non-boned van der Waals and electrostatic forces were truncated at 12 Å and smoothly switching at 10 Å. In order to accelerate the computation of MD simulations in explicit water, the parallel MD with GPU acceleration [33] was employed. After MD simulations, the stability of each protein structure was evaluated using root mean square deviation (RMSD) calculation in VMD software.

Binding free energy calculations

Molecular Mechanics Poisson-Boltzmann Surface Area approach (MM-PBSA) is computational method for calculation of binding free energy of conformational sampling along trajectory obtained from MD simulations. The method combines molecular mechanics calculations and continuum solutions models [22]. The binding free energy, $\Delta G_{binding}$, defined as:

$$\Delta G_{binding} = G_{complex} - G_{protein} - G_{ligand} \quad (1)$$

where free energies, G, of each molecule is calculated as:

$$G = E_{int} + E_{vdw} + E_{elec} + G_{PB} + G_{SA} - T\Delta S \quad (2)$$

where E_{int} is the internal molecular mechanics (bond, angle, torsion) energy, E_{vdw} and E_{elec} are the molecular van der Waals and electrostatic energy in gas-phase, respectively. G_{PB} is polar contribution of solvation energy which is calculated using APBS software [34] applying Poisson-Boltzmann finite-difference with dielectric constant value of 1 for solute and 80 for solvent. G_{SA} is non-polar contribution of solvation energy which is assumed to be proportional to the solvent accessible surface area (ASA) as following equation:

$$G_{SA} = \gamma SA + \beta \quad (3)$$

where SA is the solvent-accessible surface area, the parameterized constant values γ = 0.00542 kcal/mol.Å^2 and β = 0.92 kcal/mol. The MM-PBSA calculation is performed by the single trajectory method (STM) that both of protein trajectories are extracted from complex trajectory, the E_{int} term is zeroing out. The solute entropy (S) term is estimated by quasi-harmonic approach or by normal mode analysis [35]. This entropy calculation requires a large sampling and computationally demanding which may provide unreliable results or non-significant on a short dynamic calculation [36, 37]. Based on this consideration, we decided to ignore E_{int} and entropy terms for this calculation. All water molecule and ions were removed before calculation. To estimate the binding free energy of the simulations, the 100 snapshots have been taken with 10 ps intervals from the last 1 ns of MD trajectory. The binding energy was calculated directly for each structure of snapshot without any minimization and then the overall binding free energy ($\Delta G_{binding}$) was reported as the average values over 100 snapshots.

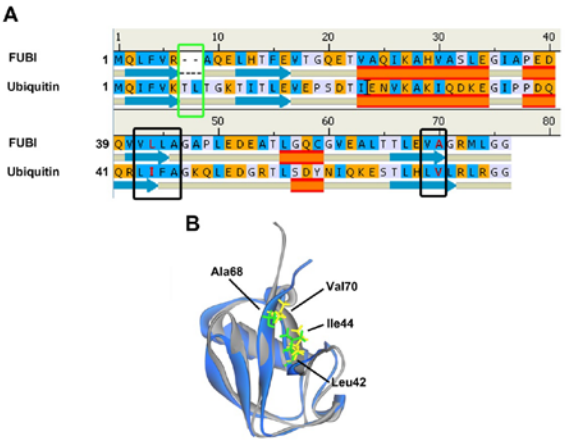

Figure 1 Sequence alignment and the superimposed structures of FUBI (PDB code: 2L7R) with ubiquitin (PDB code: 1D3Z). A) The aligned sequences of FUBI and ubiquitin with background coloring indicate the hydrophobic (blue), hydrophilic (orange) and neutral (grey) areas. The PDB type of secondary structures calculated from a linked 3D structure of FUBI and ubiquitin are displayed in cartoon and are color-coded, with helices in red, strands in blue, and coils in beige. The conserved hydrophobic residues are indicated in black boxes whereas the gap is highlighted in green box. B) The superimposed structures of FUBI with ubiquitin. The structures of FUBI and ubiquitin are shown in blue and gray ribbon, respectively. The hydrophobic key residues of FUBI and ubiquitin are depicted as green stick and yellow stick, respectively.

Binding interaction analysis of complexes

The complex structures were determined hydrophobic and H-bond interaction in 2D diagram by DIMPLOT module in LigPlot$^+$ [38]. The binding interface between two protein domains was identified and analyzed as the residues whose solvent accessible surface area is different depending on whether the protein chains are in a complex or are isolated. The computational alanine scanning was examined to predict energetically important amino acids (interaction hot spots) at the protein-protein interfaces. Both binding interface analysis and alanine scanning calculation were available in Discovery Studio 3.5. The interface binding residues within 4 Å and hydrophobic structures were detected by Discovery Studio 3.5 utility.

Computational alanine scanning

To determine the functional contribution of residues in the binding contact, *in silico* alanine-scanning mutagenesis is widely used. FUBI-p62 UBA complex was subjected to alanine-scanning mutagenesis using "Calculate Mutation Energy (Binding)" protocol of Discovery Studio 3.5 and computationally derived interaction hot spots could be identified [39]. *In silico* alanine-scanning evaluates the effect of single-point mutations on the binding affinity of protein complexes by mutating a set of selected amino-acid residues to alanine. The difference between the binding free energy of mutated structure and wild type protein provides the mutation energy ($\Delta\Delta G_{mut}$) as following equation:

$$\Delta\Delta G_{mut} = \Delta\Delta G_{bind(mutamt)} - \Delta\Delta G_{bind(wildtype)} \quad (4)$$

The binding free energy ($\Delta\Delta G_{bind}$) was calculated using CHARMm Polar H forcefield as the difference between the free energy of the complex and unbound state.

Results and Discussion

Molecular modeling analysis of FUBI and p62 UBA structures

FUBI was indicated capable of binding to the p62 UBA domain directly [6] but the data of these interactions are less known. FUBI and p62 UBA domain are members of protein family UBL (ubiquitin-like) and UBD (ubiquitin-binding domain), respectively, and several binding interactions between UBL and UBD have been investigated [19]. For FUBI binding residues, the sequence alignment of FUBI with ubiquitin and another UBL protein were carried out to examine the sequence similarity and it was suggested that FUBI has the highest homology to ubiquitin [40]. The key binding residues of ubiquitin with p62 UBA domain are Leu8, Ile44 and Val70 of which a large hydrophobic area is formed [18]. Ile44 centered on hydrophobic patch of another UBL protein was also found to play a crucial role in binding interaction with UBD [19]. In this study, 3D structures of FUBI (PDB ID: 2L7R), ubiquitin (PDB ID: 1D3Z) and p62 UBA (PDB ID: 2RRU) were analyzed. The alignment of FUBI sequence with ubiquitin sequence was obtained using Align123, a multiple sequence alignment method based on the ClustalW program. The full length of FUBI structure (Met1 to Gly74) could not be completely aligned with ubiquitin (Met1 to Gly76) because FUBI is shorter. Two gaps were added between residues Arg6 and Ala7 in FUBI according to the secondary structure visibility of FUBI and ubiquitin (Figure 1A). The final alignment showed sequence identity of 35.5% and sequence similarity of 64.5%. The regions of hydrophobic residues in FUBI were similar to the hydrophobic region of ubiquitin in which Ile44 and Val70 have been reported as important key residues for binding. The structural superimposition analysis revealed that FUBI structure was highly similar to ubiquitin. The root-mean-square deviation (RMSD) of backbone atoms was 2.9 Å. The 3D structures of FUBI and ubiquitin composed of α-helix and five β-strands. The residues Leu42 and Ala68 of FUBI were located at the same positions as Ile44 and Val70 of ubiquitin (Figure 1B). For p62 UBA domain, the key residues for binding with ubiquitin have been resolved as MGF (Met404, Gly405 and Phe406) hydrophobic patch and α-helix 3 [18, 41] (Figure 2). These binding residues are highly conserved among many other UBA domains [42, 43]. Accordingly, Leu42 and Ala68 of FUBI and Met404, Gly405, Phe406 and Gln432 of p62 UBA domain were selected as a specified set of residues at the binding interface for filtering of docking poses.

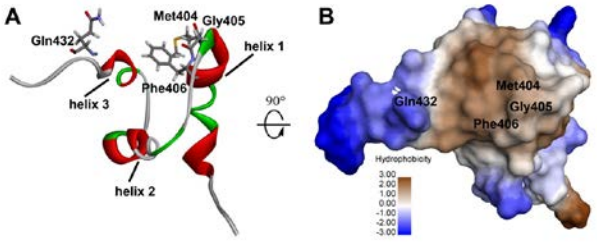

Figure 2 3D structure of p62-UBA domain in the Ub-bound state (PDB code: 2RRU). A) Ribbon structure of p62-UBA shows three-helix bundle with key residues, MGF motif and Gln432 (in stick) for ubiquitin binding. B) Surface representation of the structure of the p62-UBA domain showing the degree of hydrophobicity. The structure is viewed toward the Met-Gly-Phe (MGF motif) in the loop region and Gln432 in the C-terminus of helix 3 which is important for binding interactions with mUb.

Binding modes generated by docking of p62-UBA domain into FUBI domain

To elucidate possible binding modes of FUBI and p62 UBA, protein-protein docking technique was performed using ZDOCK program. The top 2,000 poses with high ZRANK scores were chosen from a total of 54,000 poses obtained from the docking of p62 UBA into each conformation of the FUBI NMR structure. The specified set of residues at the binding interface of FUBI (Leu42 and Ala68) and p62-UBA (Met404, Gly405 and Phe406) were used to filter the binding poses. Overall, 334 binding poses were retained. Five binding modes (I to V) of FUBI-p62 UBA complex system could be resolved using a clustering of binding poses. In this study, the specified threshold for clustering was defined by the RMSD cutoff protocol parameters; these included the maximal ligand interface RMSD of 10Å from the cluster center and a cutoff distance of 10Å to define the interface region between the two proteins. According to this clustering criterion, the cluster size of binding modes I, II, III, IV and V were 33, 42, 110, 119 and 30 poses, respectively. The structures of the predicted complexes were then refined by RDOCK calculation. The pose with the lowest RDOCK score, suggesting the most probable representing structure of that binding mode, was selected for further analysis. Figure 3 shows the results of five binding modes obtained from

docking of p62 UBA into FUBI. The different orientations of p62 UBA domain and FUBI domain of the selected docking poses are illustrated. All five binding modes, MGF hydrophobic area and helix 3 of p62 UBA domain were bound with Leu42 and Ala68 of FUBI domain. It was shown that cluster size, docking scores and visual inspection of complex poses might not be enough to conclude which of the docking pose was the optimal binding mode of FUBI-p62 UBA complex structure. Hence, to gain more understanding of FUBI-p62 UBA complex structure, molecular dynamics (MD) simulations were performed on the five possible binding modes.

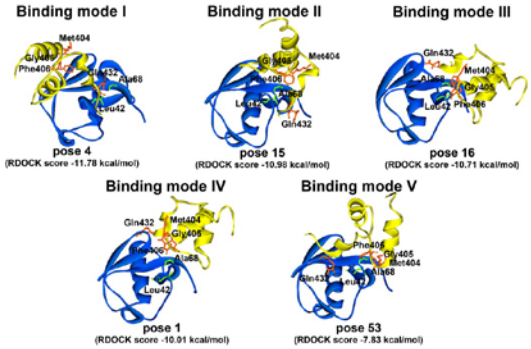

Figure 3 Differential spatial orientations of p62-UBA domain in complex with FUBI among five binding modes. The representative structure of each binding mode was obtained from the docking pose with the top RDOCK score. The MGF motif and Gln432 of p62 UBA (orange sticks), and Leu42 and Ala68 of FUBI (green sticks) using for filtering the pose are depicted and they are localized in the contact region of two proteins.

Binding mode of FUBI-p62 UBA complexes refined by MD simulations and binding free energy

Although ZDOCK was successfully used in prediction of possible binding poses of FUBI and p62 UBA, it is a rigid-body docking program, and thus not allowing their conformational changes in protein-protein interactions, protein folding and protein dynamics. In this study, MD simulations were carried out on the five structures of FUBI-p62 UBA complex systems to refine appreciative of the binding modes obtained from molecular docking. The stabilities and conformational change of the five FUBI-p62 UBA complex systems were analyzed using RMSD plots of backbone atoms during 15 ns of MD simulations. Binding pose 4 and pose 16 were stable with no RMSD fluctuations were observed during 15 ns, while pose 1, pose 15, and pose 53 were unstable with RMSD gradually increased with large fluctuation (Figure 4). The conformational changes and stabilities of the complex poses were observed during 15 ns of MD simulations. The superimposition of bound complexes from the final snapshots of the MD simulations and their initial structures are shown in Figure 4. The structural instabilities of complex pose 1, pose 15, and pose 53 were due to the distortion of the bound form after molecular dynamics (Figure 4 B, D and E). Remarkably, only high binding affinity of modes I and III were stable with RMSD remained around 2-3 Å throughout the MD simulations. The results indicated that binding mode I (pose 4) and mode III (pose 16) of complex systems were able to stay in the bound form and could be possible conformations of FUBI-p62 UBA complex. The optimal binding mode was consequently elucidated from the binding free energy calculation. The binding free energies were calculated for the complexs poses 4 and 16 using MM-PBSA methods, based on 100 snapshots taken from the last 1ns of MD trajectory. The overall binding free energy ($\Delta G_{binding}$) and all energy terms from equations (1) through (3) from the MM-PBSA method are given in Table 1. The MM-PBSA energy components of binding modes I and III revealed that electrostatic energy was the major contributor for binding energy with high polarity. The total electrostatic contribution (ΔG_{elec}) in complex system of binding modes I and III, which were composed of the gas phase electrostatice energy (ΔE_{elec}) and the polar solvation energy (ΔG_{PB}), were 6.66 and -9.46 kcal/mol, respectively. However, ΔG_{PB} of binding mode III was significantly larger compared to that of the binding mode I, with the value of 124.96 compared to 74.00 kcal/mol, respectively. This means that more desolvation energy was required for the complex system of binding mode III. Inspection of total nonpolar contribution (ΔG_{np}) clearly showed that the van der Waals energy (ΔE_{vdw}) and non-polar solvation energy (ΔG_{SA}) also facilitated the binding interactions of biding modes I and III. Overall, the complex of the binding pose 16 had the lowest binding free energy of -62.16 kcal/mol, which was around 27 kcal/mol more negative than the binding pose 4. This showed that the binding mode III of FUBI-p62 UBA complex system was more favorable than the binding mode I.

Table 1 Calculated binding free energies in terms of binding modes I and III of FUBI-p62 UBA complex (All in kcal/mol [a]).

Binding mode	ΔE_{elec}	ΔE_{vdw}	ΔG_{SA}	ΔG_{PB}	ΔG_{elec} [b]	ΔG_{np} [c]	$\Delta G_{binding}$
I (pose 4)	-67.34	-35.33	-6.34	74.00	6.66	-41.67	-35.01
III (pose 16)	-134.42	-45.01	-7.69	124.96	-9.46	-52.70	-62.16

[a] Average over 100 snapshots
[b] Total electrostatic contribution: $\Delta G_{elec} = \Delta E_{elec} + \Delta G_{PB}$
[c] Total nonpolar contribution: $\Delta G_{np} = \Delta E_{vdw} + \Delta G_{SA}$

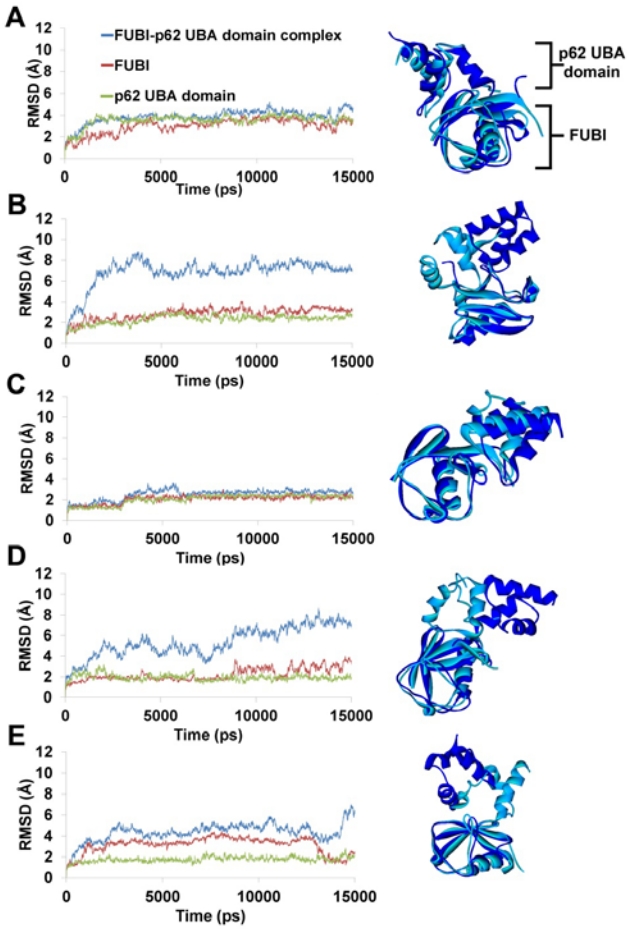

Figure 4 Stability of the five binding modes predicted from protein docking. Root mean-square deviation (Å) of backbone atoms in FUBI-p62 UBA complex from 15 ns of MD trajectories compared with starting docked structure and the superimposition of the initial (light blue) and the last snapshot (dark blue) of 3D structures.

Binding interaction analysis of FUBI-p62 UBA complex

To identify the important residues for binding interaction between FUBI and p62 UBA, the structure from the last snapshot of MD trajectory of the binding mode III complex system was analyzed. The interface binding residues in the complex structure are depicted as 3D and 2D representations shown in Figure 5. In this study, the radius of the probing sphere was set to the size of a water molecule (1.4 Å). The Solvent Accessible Surface Area (SASA) was traced out by the center of the probe when the probe rolled over the protein surface, which, in turn, was defined by the van der Waals radii of the atoms.

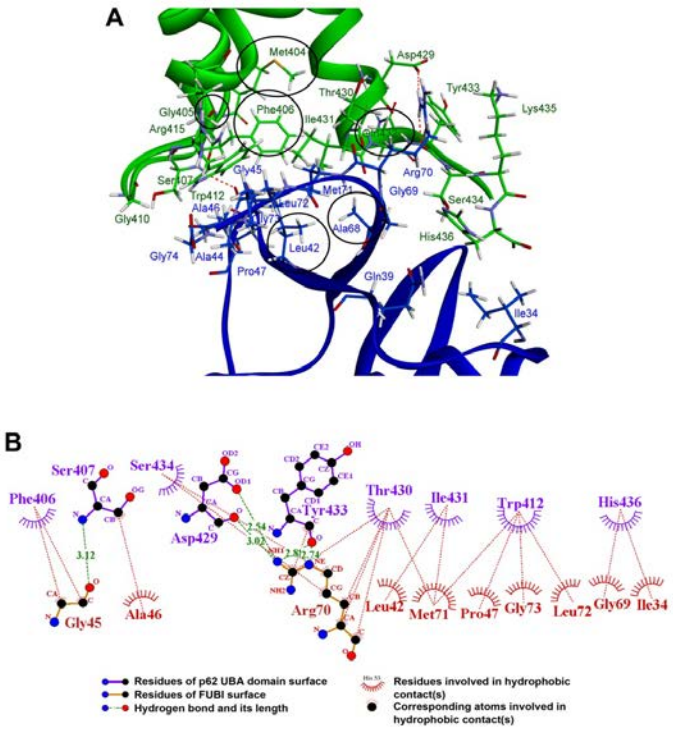

Figure 5 Plausible interactions between residues of FUBI and residues of p62 UBA domain. A) Binding interface residues between FUBI (blue) and p62 UBA (green). The MGF motif and Gln432 of p62 UBA domain and Leu42 and Ala68 of FUBI in the contact area of the complex are shown. B) 2D diagram interaction by DIMPLOT analysis. Hydrophobic interactions and hydrogen bonding patterns between FUBI and p62 UBA are illustrated.

Accordingly, the interfacing residues between FUBI and p62 UBA were identified as the residues whose solvent accessible surface area was different when the proteins were in a complex versus isolated individuals (Figure 5A).The key binding residues of p62 UBA (MGF motif and Gln432) and FUBI (Leu42 and Ala68) were found in the contact area of the complex. The residues forming hydrogen bond were illustrated. Hydrogen bonding and hydrophobic interaction between FUBI and p62 UBA domain were found by DIMPLOT analysis of the docked complex (Figure 5B). Interaction plot indicated the formation of five hydrogen bonds between two residues of FUBI and three residues of p62 UBA. Amino acids (Gly45 and Arg70) of FUBI were found to form hydrogen bonds with amino acids (Ser407, Asp429 and Tyr 433) of p62 UBA. The hydrogen bond lengths were shown to be shorter than 3.35Å for the distance between the donor and the acceptor atoms. Additionally, 8 residues (Ile34, Leu42, Ala46, Pro47, Gly69, Met71, Leu72 and Gly73) of FUBI were involved in hydrophobic

interaction with 6 amino acids (Phe406, Trp412, Thr430, Ile431, Ser434 and His 436) of p62 UBA. The computation based alanine-scanning mutagenesis of FUBI-p62 UBA complex was performed in order to compute for mutation energy for alanine substitution at each position. The mutation energy based on the effect of the respective mutation on binding stability was determined (Table 2). The FUBI residues (Leu42, Pro47, Arg70 and Met71) with destabilizing effect upon alanine mutation were considered as hot spot residues for p62 UBA domain interaction. For p62 UBA domain, the hotspot residues for FUBI interaction were Phe406 Trp412, Arg415, Thr430, Ile431 Lys435 and His 436 which were destabilized upon alanine mutation. The results also revealed that residues Leu42, Pro47 and Met71 of FUBI and Phe406, Trp412, Thr430, Ile431 and His 436 of p62 UBA were consistently involved in hydrophobic binding interactions. Moreover, the residue Arg70 of FUBI is involved in hydrogen bonding with Asp429 and Tyr433 of p62 UBA, thus confirmed theirs significance as key interacting residues.

Conclusion

In this work, a plausible structure of FUBI in complex with p62 UBA domain was obtained by a combination of computational methods including ZDOCK, RDOCK, MD simulations and MM-PBSA binding free energy calculation. Five possible binding modes were exhibited with different orientations of p62 UBA domain with respect to FUBI. However, only two binding mode structures were stable after 15 ns of MD simulations and their MM-PBSA binding energies were calculated to indicate the best FUBI-p62 UBA complex structure. Our study thus provides an insight into the structural information of the binding interaction between p62 and Fau which is a crucial step of autophagy-targeting p62 mechanism for the antimycobacterial action.

Table 2 Computational alanine scanning mutagenesis of FUBI-p62 UBA complex

FUBI			**p62 UBA domain**		
Mutation	Mutation Energy (kcal/mol)	Effect	Mutation	Mutation Energy (kcal/mol)	Effect
I34A	0.47	neutral	F406A	1.03	destabilizing
Q39A	0.39	neutral	S407A	-0.37	neutral
L42A	0.98	destabilizing	G410A	-0.35	neutral
G45A	-0.48	neutral	W412A	3.03	destabilizing
P47A	1.56	destabilizing	R415A	1.23	destabilizing
G69A	-0.21	neutral	D429A	-0.35	neutral
R70A	2.95	destabilizing	T430A	0.87	destabilizing
M71A	0.76	destabilizing	I431A	0.95	destabilizing
L72A	0.18	neutral	Y433A	-0.09	neutral
G73A	-0.16	neutral	S434A	-0.4	neutral
G74A	-0.04	neutral	K435A	0.87	destabilizing
G405A	-0.09	neutral	H436A	0.93	destabilizing

Acknowledgements

The authors are very grateful to the National Research University Grant (NRU-PY540106) for the financial support.

References

[1] I. Vergne, J. Chua, S.B. Singh and V. Deretic. Cell biology of *Mycobacterium tuberculosis* phagosome, *Annu. Rev. Cell Dev. Biol.* 20: 367-94 (2004).

[2] J.A. Armstrong and P.D. Hart. Phagosome-lysosome interactions in cultured macrophages infected with virulent tubercle bacilli, *J. Exp. Med*. 142: 1-16 (1975).

[3] R.A. Fratti, J. Chua, I. Vergne and V. Deretic. *Mycobacterium tuberculosis* glycosylatedphosphatidylinositol causes phagosome maturation arrest, *P. Natl. Acad. Sci. USA*. 100: 5437-42 (2003).

[4] M.G. Gutierrez, S.S. Master, S.B. Singh, G.A. Taylor, M.I. Colombo and V. Deretic. Autophagy Is a Defense Mechanism Inhibiting BCG and *Mycobacterium tuberculosis* Survival in Infected Macrophages, *Cell*. 19: 753-66 (2004).

[5] S. Alonso, K. Pethe, D.G. Russell and G.E. Purdy. Lysosomal killing of *Mycobacterium* mediated by ubiquitin-derived peptides in enhanced by autophagy, *P. Natl. Acad. Sci. USA*. 104: 6031-6 (2007).

[6] M. Ponpuak, A.S. Davis, E.A. Roberts, M.A. Delgado, C. Dinkins, Z. Zhao, H.W. Virgin IV, G.B. Kyei, T. Johansen, I. Vergne and V. Deretic. Delivery of cytosolic components by autophagic adaptor protein p62 endows autophagosomes with unique antimicrobial properties, *Immunity*. 32: 329-41 (2010).

[7] C. He and D.J. Klionsky. Regulation mechanisms and signaling pathways of autophagy, *Annu. Rev. Genet*. 43: 67-93 (2009).

[8] N. Mizushima, B. Levine, A.M. Cuervo and D.J. Klionsky. Autophagy fights disease through cellular self-digestion, *Nature*. 451: 1069-75 (2008).

[9] Y.T. Zheng, S. Shahnazari, A. Brech, T. Lamark, T. Johansen and J.H. Brumell. The adaptor protein p62/SQSTM1 targets invading bacteria to the autophagy pathway, *J. Immunol*. 183: 5909-16 (2009).

[10] N. Dupont, S. Lacas-Gervais, J. Bertout, I. Paz, B. Freche, G.T. Van Nhieu, F.G. van der Goot, P.J. Sansonetti and F. Lafont. Shigella phagocytic vacuolar membrane remnants participate in the cellular response to pathogen invasion and are regulated by autophagy, *Cell Host Microbe*. 6: 137-49 (2009).

[11] Y. Yoshikawa, M. Ogawa, T. Hain, M. Yoshida, M. Fukumatsu, M. Kim, H. Mimuro, I. Nakagawa, T. Yanagawa, T. Ishii, A. Kakizuka, E. Sztul, T. Chakraborty and C. Sasakawa. Listeria monocytogenes ActA-mediated escape from autophagic recognition, *Nat. Cell Biol*. 11: 1233-40 (2009).

[12] T.L. Thurston, G. Ryzhakov, S. Bloor, N. von Muhlinen and F. Randow. The TBK1 adaptor and autophagy receptor NDP52 restricts the proliferation of ubiquitin-coated bacteria, *Nat. Immunol*. 10: 1215-21 (2009).

[13] A. Orvedahl, S. MacPherson, R. Sumpter Jr, Z. Tallóczy, Z. Zou and B. Levine. Autophagy protects against Sindbis virus infection of the central nervous system, *Cell Host Microbe*. 7: 115-27 (2010).

[14] C. Dinkins, J. Arko-Mensah and V. Deretic. Autophagy and HIV, *Semin. Cell Dev. Biol*. 21: 712-8 (2010).

[15] S.J. Howell, D. Wilk, S.P. Yadav and C.L. Bevins. Antimicrobial polypeptides of the human colonic epithelium, *Peptides*. 24: 1763-70 (2003).

[16] M. Tollin, P. Bergman, T. Svenberg, H. Jornvall, G.H. Gudmundsson and B. Agerberth. Antimicrobial peptides in the first line defence of human colon mucosa, *Peptides*. 24; 523-30 (2003).

[17] J. Olvera and I.G. Wool. The carboxyl extension of a ubiquitin-like protein is rat ribosomal protein S30, *J. Biol. Chem*. 268: 17967-74 (1993).

[18] S. Isogai, D. Morimoto, K. Arita, S. Unzai, T. Tenno, J. Hasegawa and *et al.* Crystal structure of the ubiquitin-associated (UBA) domain of p62 and its interaction with ubiquitin, *J. Biol. Chem*. 286: 31864-74 (2011).

[19] J.M. Winget and T. Mayor. The Diversity of Ubiquitin Recognition:Hot Spots and Varied Specificity, *Mol. Cell*. 38: 627-35 (2010).

[20] Accelrys Software Inc., *Discovery Studio Modeling Environment, Release 3.5*, San Diego: Accelrys Software Inc., (2007).

[21] K. Wiehe, B. Pierce, J. Mintseris, W.W. Tong, R. Anderson, R. Chen and Z. Weng. ZDOCK and RDOCK Performance in CAPRI Rounds 3, 4, and 5, *Proteins*. 60: 207-13 (2003).

[22] I. Massova and P.A. Kollman. Combined molecular mechanical and continuum solvent approach (MM-PBSA/GBSA) to predict ligand binding, *Perspect. Drug Discov*. 18: 113-35 (2000).

[23] R. Chen, W. Tong, J. Mintseris, L. Li and Z. Weng. ZDOCK predictions for the CAPRI challenge, *Proteins.* 52: 68-73 (2003).

[24] R. Chen and Z. Weng. A novel shape complementarity scoring function for protein-protein docking, *Proteins*. 51: 397-408 (2003).

[25] B. Pierce and Z. Weng. ZRANK: Reranking Protein Docking Predictions with an Optimized Energy Function, *Proteins*. 67: 1078-86 (2007).

[26] L. Li, R. Chen and Z.P. Weng. RDOCK: Refinement of rigid-body protein docking predictions, *Proteins*. 2003; 53, 693-707.

[27] J.C. Phillips, R. Braun, W. Wang, J. Gumbart, E. Tajkhorshid, E. Villa, C. Chipot, R.D Skeel, L. Kale and K. Schulten. Scalable molecular dynamics with NAMD, *J. Comput. Chem*. 26: 1781-802 (2005).

[28] A.D. MacKerell Jr, B.R. Brooks, C.L. Brooks III, L. Nilsson, Y. Won, M. Karplus, CHARMM: the energy function and its parameterization with an overview of the program. In: P von Rague Schleyer (ed.), *The Encyclopedia of Computational Chemistry*, John Wiley & Sons, New York, 1998.
[29] W.L. Jorgensen, J. Chandrasekhar, J.D. Madura, R.W. Impey and M.L. Klein. Comparison of simple potential functions for simulating liquid water, *J. Chem. Phys*. 79: 926-35 (1983).
[30] W.F. Van Gunsteren, H.J.C. Berendsen. Algorithms for macromolecular dynamics and constraint dynamics, *Mol. Phys*. 34: 1311-27 (1977).
[31] G.J. Martyna, D.J. Tobias and M.L. Klein. Constant pressure molecular dynamics algorithms, *J. Chem. Phys*. 101: 4177-89 (1994).
[32] T. Darden, D. York and L. Pedersen. Particle mesh Ewald: An *N*·log(N) method for Ewald sums in large systems, *J. Chem. Phys*. 98: 10089-92 (1993).
[33] J.E. Stone, J.C. Phillips, P.L. Freddolino, D.J. Hardy, L.G. Trabuco, K. Schulten. Accelerating molecular modeling applications with graphics processors, *J. Comp. Chem*. 28: 2618-64 (2007).
[34] N.A. Baker, D. Sept, S. Joseph, M.J. Holst and J.A. McCammon. Electrostatics of nanosystems: Application to microtubules and the ribosome, *P. Natl. Acad. Sci. USA*. 98: 10037-41 (2001).
[35] H. Gohlke and D.A. Case. Converging free energy estimates: MM-PB(GB)SA studies on the protein-protein complex ras-raf, *J. Comput. Chem*. 25: 238-50 (2004).
[36] S.P. Brown and S.W. Muchmore. Large-scale application of high-throughput molecular mechanics with poisson-boltzmann surface area for routine physicsbased scoring of protein-ligand complexes, *J. Med. Chem*. 52: 3159-65 (2009).
[37] R. Majumdar, R. Railkar and R.R. Dighe. Docking and free energy simulations to predict conformational domains involved in hCG-LH receptor interactions using recombinant antibodies, *Proteins*. 79: 3108-22 (2011).
[38] R.A. Laskowski and M.B. Swindells. LigPlot+: multiple ligand-protein interaction diagrams for drug discovery, *J. Chem. Inf. Model*. 51: 2778-86 (2011).
[39] V.Z. Spassov, L. Yan and S.Z. Szalma. Introducing an implicit membrane in Generalized Born/solvent accessibility continuum solvent models, *J. Phys. Chem. B.* 106: 8726-38 (2002).
[40] T.G. Rossman, M.A. Visalli1 and E.V. Komissarova. fau and its ubiquitin-like domain (FUBI) transforms human osteogenic sarcoma (HOS) cells to anchorage-independence, *Oncogene*. 22: 1817-21 (2003).
[41] J. Long, T.R.A. Gallagher, J.R. Cavey, P.W. Sheppard, S.H. Ralston, R. Layfield and *et al*. Ubiquitin recognition by the ubiquitin-associated domain of p62 involves a novel conformational switch, *J. Biol. Chem*. 283: 5427-40 (2008).
[42] A. Ohno, J. Jee, K. Fujiwara, T. Tenno, N. Goda, H. Tochio and *et al*. Structure of the UBA domain of Dsk2p in complex with ubiquitin molecular determinants for ubiquitin recognition, *Structure*. 13: 521-32 (2005).
[43] Y.G. Chang, A.X. Song, Y.G. Gao, Y.H. Shi, X.J. Lin, X.T. Cao and *et al*. Solution structure of the ubiquitin-associated domain of human BMSC-UbP and its complex with ubiquitin, *Protein Sci*. 15: 1248-59 (2006).